IEEE Access
Multidisciplinary | Rapid Review | Open Access Journal

Received September 20, 2021, accepted October 16, 2021, date of publication October 25, 2021, date of current version November 4, 2021.

Digital Object Identifier 10.1109/ACCESS.2021.3122535

An Active Contour Method Based on Regularized Kernel Fuzzy C-Means Clustering

SHAFIULLAH SOOMRO[1], (Member, IEEE), ASAD MUNIR[2], (Member, IEEE), ASIF AZIZ[1], (Member, IEEE), TOUFIQUE AHMED SOOMRO[3], (Member, IEEE), AND KWANG NAM CHOI[1], (Member, IEEE)

[1]Department of Computer Science and Engineering, Chung-Ang University, Seoul 06974, South Korea
[2]Department of Industrial and Information Engineering, University of Udine, 33100 Udine, Italy
[3]School of Computing and Mathematics, Charles Sturt University, Bathurst Campus, Bathurst, NSW 2795, Australia

Corresponding author: Kwang Nam Choi (knchoi@cau.ac.kr)

This work was supported in part by the National Research Foundation of Korea (NRF) funded by the Korean Government Ministry of Science and Information Technology (MSIT) under Grant 2019R1F1A1062612, and in part by the Ministry of Science and ICT and NIPA through the HPC Support Project.

ABSTRACT This research presents hybrid level set evolution for complex and inhomogeneous image segmentation. Firstly, we develop an adaptive force with level set evolution, which is driven by region information. Adaptive force is produced by consolidating local and global force terms in an altered fashion. Besides, to avoid local fitting terms being stuck into a local minimum, we use the swap function to interchange the fitting terms so that fitting values inside the object are always higher. Later for the elimination of the costly contour initialization that existed in previous level set based evolutions, we integrate kernel based fuzzy c-means clustering and intensity-based thresholding framework with the proposed framework to automate the proposed strategy. Finally, for the level set function regularization and the for the elimination of its re-initialization we have used the Gaussian function in the level set evolution. We demonstrate the results on some complex images to show the strong and exact segmentation results that are conceivable with this new class of adaptive active contour model. We have additionally performed statistical analysis on real images and BRATS dataset using Dice index, accuracy, sensitivity, specificity and Jaccard index metrics. Results show that the proposed method gets high Dice index, accuracy, sensitivity, specificity and Jaccard index values compared to the previous state of art methods.

INDEX TERMS Active contours, bias field, level set, clustering.

I. INTRODUCTION

A n Image segmentation is a significant stage in computer vision and image processing applications [1]. Inhomogeneity or pixel variation is one of the striking issues in image segmentation, which emerges from the flaws that occurred during the image obtaining process or because of outside obstructions. It appears as a smooth variation of pixels that causes problem during segmentation process. For instance, in clinical imaging, these weaknesses could prompt some unacceptable choice of image boundaries. Thusly, the complexity of inhomogeneity can incite counterfeit results that can be hard for experts and radiologists to decide actual outcome [2].

In the context of Image segmentation, active contours have been profoundly used [3]–[6], which have ended up being incredibly well known and have found applications in numerous image segmentation applications. The core idea is to allow a curve to deform using the energy minimizing principle. Two significant classes that exist for active contours are edge-based [7]–[9] and region-based [10], [11], [17]–[19], [21], [22], [24]–[28], [30], [31].

Edge related contours use gradient data to perceive object boundaries. However, gradient information is not adequate in all circumstances. Moreover, this technique is very fragile to noisy image data and extraordinarily dependent on contour initial position. One preferred benefit of this sort of plan is that there should be no region based constraints considered for this kind of technique. Consequently, the correct segmentation can be achieved in specific instances for diverse or homogeneous intensity images.

The associate editor coordinating the review of this manuscript and approving it for publication was Essam A. Rashed.

On the other hand, region based level set methods are based on pixel information inside an image. These approaches distinguish the background and foreground in a quantifiable manner and build up a vital energy function. Among all region based techniques, some comprehensively used regional global models and presumes the image regions as homogeneous or constant [10], [11]. Further, few of the eminent region based methods are local, which overthrow the issues of the global active contours and consider localized data of an image for inhomogeneous image segmentation [22].

The corresponding segmentation of edge and region active contours is appeared in Fig 1, where (a) expresses the outcome of LSEWR (level set evolution without re-initialization) [9] technique, (b) expresses the result of the Chan-Vese [11] and (c) expresses the result of the LBF (Local Binary Fitting) [9]. This may be reasoned from Fig 1 that, local energy active contours have some capacity to deal with inhomogeneities to some extent. Nevertheless, localized active contours are not constantly adequate to accomplish precise image segmentation. Despite various intensity based contour techniques, inhomogeneous image segmentation is as yet a current issue in this research area, which occurs from unsatisfactory image obtainment procedures or from the outside impedance. It has been seen that the bias field is likewise utilized as a first step for achieving better segmentation results. So far, various bias correction segmentation strategies have been also proposed in this context [3], [5], [5]. However, these methods have been found insufficient to segment object due to the occurrence of only local energy functionals.

A local energy functional model was proposed by Zhang *et al.* in [24]. This method has described the local image fitting (LIF) model by utilizing localized intensity information. In this method, the force term was developed as a subtractive term between the original and fitted image. In addition, the Gaussian kernel is used to direct the level-set function stability after each cycle.

In [16], a unique region based active contour scheme is given by utilizing a global signed pressure force (SPF) function. The SPF force term is characterized by utilizing intensity means taken from [11].

In [3], [34] force term was proposed, which has infused bias estimation and correction in the context of inhomogeneous segmentation. This model has portrayed force that segments an object by minimizing the energy formulation and performs bias field estimation altogether.

Lately, hybrid active contours [17]–[21], [28], [35] have been exceptionally well known for segmentation. These models consolidate region-edge data in an alternate fashion dependent on various applications. In this context, Soomro *et al.* [20] proposed a hybrid technique, which coordinates region and edge data in an additive fashion. This technique unites region and edge force terms, which produces improved segmentation results.

This research proposes a novel active contour strategy with the subsequent contributions.

1) Firstly, this method develops hybrid energy functionals based on a local and global image model.
2) Local and Global force terms are formulated and combined to form an adaptive force, which accomplishes inhomogeneous image segmentation.
3) Local fitting terms are swapped by using swap function to avoid contour being trapped in a local minimum.
4) A kernel base fuzzy c-means clustering and Intensity based thresholding is used as an initialization stage, which makes the proposed algorithm robust and consistent.

The proposed method has been carried out over various images including the BRATS dataset and compared with previous research. Results will verify that the proposed strategy offers a better approach and accomplish required segmentation results with high accuracy in contrast to previous methods.

The next steps of the proposed research are as follows. The background literature is depicted in segment II. The proposed method is clarified in III. Exploratory and results investigations are portrayed in segment IV. Quantitative descriptions are introduced in segment V using skin lesion and BRATS dataset.Discussion is explained in VI. Finally, the conclusion is portrayed in segment VII.

II. BACKGROUND

A. CHAN-VESE MODEL

Chan-Vese [11] foreseen a progressively fathomable formulation containing an idea of Mumford and Shah model [10]. By estimating the image intensity forces inside and outside of curve, Chan-Vese computes forces known as j_1 and j_2 separately. Let an image be represented as $I : \Omega \subset R^2$, level set as $\phi : \Omega \subset R^2$ and curve C is zero level set: $C = \{x \in \Omega | \phi(x) = 0\}$. The energy formulation of Chan-Vese strategy defined as:

$$\begin{aligned} E_{CV}(C, j_1, j_2) = \lambda_1 \int_{\Omega} |I(x) - j_1|^2 H_\varepsilon(\phi(x)) dx \\ + \lambda_2 \int_{\Omega} |I(x) - j_2|^2 (1 - H_\varepsilon(\phi(x))) dx \\ + \mu \int_{\Omega} |\nabla H_\varepsilon(\phi)|^2 dx + \nu \int_{\Omega} H_\varepsilon(\phi) dx \end{aligned} \quad (1)$$

where $\mu \geq 0$, $\nu \geq 0$ and $\lambda_1, \lambda_2 \geq 0$, are scaling constants where $\mu \geq 0$ balances the length term and ν balances the region term for curve C individually. $H_\varepsilon(\phi)$ is the Heaviside term composed as:

$$H_\varepsilon(\phi) = \frac{1}{2}\left(1 + \frac{2}{\pi} \arctan\left(\frac{\phi}{\varepsilon}\right)\right) \quad (2)$$

ϵ stabilize the smoothness of Heaviside term. Two forces j_1 and j_2 in Eq (1), describe globally approximated terms across the curve C. By getting derivative of Eq (1), with respect to ϕ using [36], the proportionate level set energy

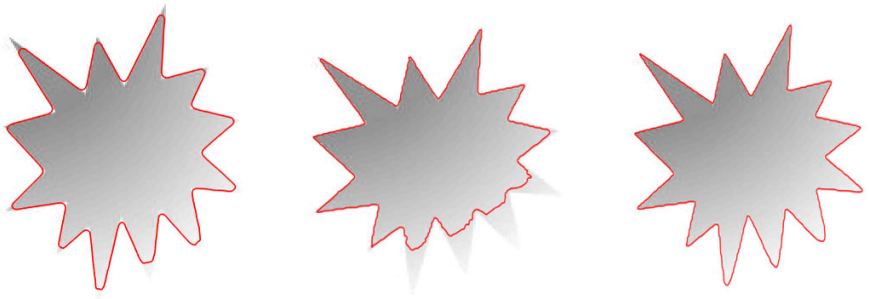

FIGURE 1. Previous methods segmentation. a: Result of LSEWR [9]; b: Outcome of Chan-Vese [11]; c: Outcome of the LBF [22].

functional is composed as follows.

$$\frac{\partial \phi}{\partial t} = \left(-\lambda_1(I-j_1)^2+\lambda_2(I-j_2)^2+\mu div\left(\frac{\nabla\phi}{|\nabla\phi|}\right)-v\right)\delta_\varepsilon(\phi) \tag{3}$$

$\delta_\epsilon(\phi)$ defined as a Dirac delta function, described as:

$$\delta_\varepsilon(\phi) = \frac{\varepsilon}{\pi(\phi^2+\varepsilon^2)} \tag{4}$$

Besides scaling the value of the Heaviside term in Eq (2), ϵ also adjusts the width of a Dirac delta term in Eq (4). Keeping ϕ fixed and minimization of Eq (1), for j_1 and j_2, we get the following details:

$$j_1 = \frac{\int_\Omega I(x)H_\varepsilon(\phi(x))dx}{\int_\Omega H_\varepsilon(\phi(x))dx}$$
$$j_2 = \frac{\int_\Omega I(x)(1-H_\varepsilon(\phi(x)))dx}{\int_\Omega (1-H_\varepsilon(\phi(x)))dx} \tag{5}$$

The final energy in Chan-Vese strategy is related solely to global intensity for an image inside and outside of the curve C. Therefore, this strategy creates an inappropriate outcome if the image has a localized or inhomogeneous force locales.

B. LOCAL BINARY FITTED MODEL

Li *et al.* [22] foreseen (LBF) local binary fitting strategy to manage inhomogeneity issue by coupling an image local pixel data into their formulations. Let us accept an image $I : \Omega \subset R^2$, a level set $\phi : \Omega \subset R^2$, and a curve as C. The proposed energy term is characterized as:

$$E_{LBF}(C,f_1,f_2) = \lambda_1\int_\Omega K_\sigma(x-y)|I(y)-f_1(x)|^2H_\epsilon(\phi(y))dy + \lambda_2\int_\Omega K_\sigma(x-y)|I(y)-f_2(x)|^2(1-H_\epsilon(\phi(y)))dy \tag{6}$$

where some parameters are λ_1, $\lambda_2 \geq 0$ and $H_\varepsilon(\phi)$ is the Heaviside function clarified in Eq (2). $f_1(x)$ and $f_2(x)$ are local forces determined from the two sides of curve C, which are characterized as.

$$f_1(x) = \frac{K_\sigma * [H_\epsilon(\phi)I(x)]}{K_\sigma * H_\epsilon(\phi)} \tag{7}$$
$$f_2(x) = \frac{K_\sigma * [(1-H_\epsilon(\phi))I(x)]}{K_\sigma * (1-H_\epsilon(\phi))} \tag{8}$$

Furthermore, the length term is additionally incorporated for the regularization of the level set ϕ. The numerical detailing of this procedure is composed as:

$$\frac{\partial\phi}{\partial t} = -\delta_\varepsilon(\phi)\lambda_1\int_\Omega K_\sigma(x-y)|I(x)-f_1(y)|^2dy - \lambda_2\int_\Omega K_\sigma(x-y)|I(x)-f_2(y)|^2dy(-\delta_\varepsilon) + v\delta_\varepsilon(\phi)div\left(\frac{\nabla(\phi)}{|\nabla(\phi)|}\right)+\mu\left(\Delta\phi-div\left(\frac{\nabla\phi}{|\nabla\phi|}\right)\right) \tag{9}$$

In above formulation, μ is to tune regularization term and v is a parameter for length term, which helps curve to move towards image boundaries. K_σ is a Gaussian window term with standard deviation characterized as:

$$K_\sigma(x-y) = \frac{1}{(2\pi)^{n/2}\sigma^n}\exp\left(-\frac{|x-y|^2}{2\sigma^2}\right) \tag{10}$$

σ is for Gaussian standard deviation used to adjust the local property of LBF model, which can be taken for smaller local space or for the entire image local space.

The consideration of Gaussian function ponders an image local pixel force data inside the two sides of curve C and grants leverage to this strategy to catch objects with inhomogeneity. Moreover, local pixel data is not in every case enough to complete an exact segmentation process. Moreover, this strategy is horrendously sensitive to the initial curve and stuck into local minima if we initialize it away from image boundaries.

C. LOCAL IMAGE FITTED (LIF) MODEL

This model was proposed [24] a subtractive fitted model in their formulation. The formulation of this strategy is:

$$E_{LIF} = \frac{1}{2}\int_{\Omega} |I(x) - I_{LIF}(x)|^2 dx, \tag{11}$$

I_{LFI} is locally fitted image defined as:

$$I_{LIF}(x) = f_1(x)H_\epsilon(\phi) + f_2(x)(1 - H_\epsilon(\phi)) \tag{12}$$

where both f_1 and f_2 are localized forces characterized in Eq (7) and Eq (8). $H_\epsilon(\phi)$ is Heaviside term characterized in Eq (2). Utilizing standard gradient decent strategy [36], minimization of Eq (11) regarding ϕ acquire these details.

$$\frac{\partial \phi}{\partial t} = (I(x) - I_{LIF}(x))(f_1(x) + f_2(x))\delta_\varepsilon(\phi) \tag{13}$$

D. VLSBCS MODEL

As of late, Li *et al.* [3], [34] conceived a(VLSBCS) variational level-set strategy for the segmentation and bias rectification. This technique relies upon retinex model, which explain images having inhomogeneity, described as:

$$I(x) = b(x)J(x) + n(x), \tag{14}$$

The equation above represents *I(x)* as an image with inhomogeneities, *J(x)* is the image to be restored from inhomogeneities, *b(x)* is the bias field that is liable for inhomogeneities and *n(x)* is noise in the image. This strategy takes retrieved image *J(x)* as a smooth inside each region in an image. This idea technically formulated as:

$$J(x) \approx \sum_{i=1}^{N} c_i M_i \; for \; x \in \Omega_i \; with \; x \in \{\Omega_i\}_{i=1}^{N}, \tag{15}$$

This strategy utilizes K-means to group neighborhood image forces. K-implies use iterative method to minimize the following target function:

$$E \cong \int \left(\sum_{i=1}^{N} \int_{\Omega i} K_\sigma(x - y)|I(y) - b(x)c_i|^2 dy \right) dx \tag{16}$$

where $b(x)$ is the bias field defined in Eq (18) and c_i is local pixel intensity. For the single level set approach the estimation of i will be $i = 2$. On account of single-phase level set based active contour, taking derivative of the above formulation with respect to $\{\Omega_i\}_{i=1}^{N}$. We have two regions Ω_1, Ω_2 represents by zero level set $\Omega_1 \cong \phi > 0$ and $\Omega_2 \cong \phi < 0$. We have final energy functional as:

$$E = \int \left(\sum_{i=1}^{N} \int_{\Omega i} K_\sigma(x - y)|I(y) - b(x)c_i|^2 M_i(\phi) dy \right) dx, \tag{17}$$

where M_i represents Heaviside term and for single phase level set strategy we take $M_1 = H(\phi)$ and $M_2 = (1 - H(\phi))$. By getting the derivative of E, we get the undermentioned equations for $b(x)$ and c_i.

$$b(x) = \frac{\sum_{i=1}^{2} K_\sigma * \left[I(x)c_i M_i(\phi)\right]}{\sum_{i=1}^{2} K_\sigma * \left[c_i^2 M_i(\phi)\right]} \tag{18}$$

$$c_i = \frac{\int K_\sigma * \left[I(x)b(x)M_i(\phi)\right] dx}{\int K_\sigma * \left[b^2(x)M_i(\phi)\right] dx} \tag{19}$$

E. WANG et al MODEL

In [35], proposed the adaptive level set force, which can adaptively move contour direction as up or down as per image data. They propose the final energy functional as follows:

$$E(I, j_1, j_2) = sign\left(I(x, y) - \frac{j_1 + j_2}{2} \right) \tag{20}$$

where j_1 and j_2 are global intensity forces taken from Eq (5) respectively.

In this method the level set function has essentially introduced as a constant value instead of the generally utilized signed distance function adapted in existing level set models. Thus, this model totally dispenses the necessities of initial contour, thus eliminates the issues that came because of initial curve initialization. The level set evolution of this method is as follows:

$$E_{adp}(I, \phi) = g(|\nabla I_\sigma|) sign\left(I(x, y) - \frac{j_1 + j_2}{2} \right) \tag{21}$$

III. PROPOSED HYBRID ENERGY FUNCTIONAL

To address inhomogeneity, a multiplied model is being taken for the bias field approximation. Therefore, this research takes multiplicative retinex model clarified in Eq (14), where *J(x)* is believed to be built up by smooth image intensities i-e., *k*. *I(x)* would in this way be formulated as:

$$I(x) = b(x)\{c_1 M_1 + c_2 M_2 + \ldots\ldots c_k M_k\} \tag{22}$$

where force implies c_i determined for relating region $\{\Omega_i\}_{i=1}^{N}$ and M_i is the attribute of each region.

We propose an adaptive level set function as,

$$E_{Adp} = \alpha sign\left(E_{force}(\phi) \right) + \nu A_{Adp}(\phi) \tag{23}$$

where α and ν are controlling parameters for adaptive energy and area term.

$E_{force}(\phi)$ is an adaptive driving force of local and global energy, which operates the movement of the level set function. Defined as:

$$E_{force} = \big(I(x)\text{-}(1 - w)\big(b(x)\big)(c_1) - w(J_1)\big) + \big(I(x)\text{-}(1 - w)(b(x))(c_2) - w(J_2)\big) \tag{24}$$

The scaling parameter w is used to modify the model for intensity variation. w is picked close to 1 if an image has greater variations or inhomogeneities and w is picked close to 0 for images, which have smooth or homogeneous

regions. Eq (23) area term $A(\phi)$ accelerates the curve evolution, written as.

$$A(\phi) = v \int H_\epsilon(-\phi) \tag{25}$$

c_1 and c_2 are taken as local intensity means from Eq (19). $b(x)$ is a bias estimation field taken from Eq (18) and j_1 and j_2 are global means explained in Eq (5).

It has been observed that, local energy models are very sensitive to contour position, in this regard we have also addressed and tried to improve local energy model with little improvement. It has been noticed that, to acquire the required object segmentation the contour position is to be considered near the object boundary and the value of c_2 (inside object) should be greater than c_1 (outside object). To make this happen, we have formulated a swap function inside our framework, this function will check the values of both c_1 and c_2 near the object and interchanges it in that region. This phenomenon is described in Fig 2.

Swap function comprises of min and max functions to interchange local intensity values of c_1 and c_2 taken from Eq (19), these functions are mathematically described as:

$$\begin{aligned} {c_1}^* &= \min(c_1, c_2) \\ {c_2}^* &= \max(c_1, c_2) \end{aligned} \tag{26}$$

The global force terms characterized in Eq (24) have only help contour to move away from the boundary and assist local force to capture inhomogeneous regions smoothly. Hybrid active contours have been defined in detailed perspective [17], [18], [21], [24], some of them join global forces and others utilizing localized imperatives. The new force proposed in this research relies on global and local intensity forces. Fig 3 shows how global and local force intermingle during level set evolution.

Global intensity forces are not satisfactory to complete the image segmentation process having inhomogeneity. Similarly, models dependent on the merely local forces have many computational and time complications. Adapting local and global fitted forces, the proposed system can deal with the inhomogeneity issue without causing any hindrances. Further, it has been additionally seen that models with merely global forces cannot catch objects with inhomogeneity because global models are built up under the supposition of homogeneous pixel regions.

Taking the derivative of the proposed method's energy functional E_{Adp} from Eq (23) by using gradient descent method [36], the final level set equation is:

$$\frac{\partial \phi}{\partial t} = \Big(\alpha E_{Adp}(\phi)) - v\Big)\delta_\varepsilon \tag{27}$$

In this research, adaptive force is designed, which changes its sign itself. Therefore, we initialize the level set function as a constant function for all the images defined as:

$$\phi(x, t = 0) = \rho \quad x \in \Omega \tag{28}$$

TABLE 1. Experiment and validation values used in results.

Symbol	Quantity	Parameter value
α	Adaptive force parameter	0.4
v	Area term	$0.00001 * 255 * 255$
σ	Gaussian kernel parameter	0.3
ρ	Initial level set constant	2
ϵ	Dirac constant	1.5
∇	Time-step	0.1
w	w parameter	0.001

$\rho \geq 0$ is an any constant value. In the end, the iterative steps of the proposed strategy are followed as algorithm below:

Algorithm

1) **Initialize** level set as constant function,$\phi(x, t = 0)$ in Eq (28).
2) $n = 1$.
3) **while** curve evolution is not completed **do**
4) Find global and local intensities from Eq (5) and from Eq (26).
5) Find the bias value Eq (18),
6) Solve the final level set using Eq (27).
7) $n = n + 1$.
8) **end while**
9) **Output:** Converged outcome, ϕ.

IV. RESULTS AND DISCUSSION

Each observation is executed in MATLAB 2019 on a Windows 10 in a PC with Intel i7, 2.9 GHz with 16 GB RAM. The values for proposed technique are documented in Table 1.

The initial result is displayed in Fig 4, which explains the working principle of the proposed approach over inhomogeneous image. The initialization curve is shown in (a), the bias field and the corrected image is shown in (b), (c) and the final outcome of the proposed method is shown in (d).

To check the consistency of the proposed method, we used some images, which are common for almost all previous methods. The result of the proposed method and its comparison is shown in Fig 5. Column VII reflects the results of the proposed method, which is consistent and robust against previous methods.

Further, we used images from a publicly available dataset for assessing the quality of the proposed method and its comparison with other methods. The results of the proposed and previous methods are depicted in Fig 6, where the proposed method has surpassed existing methods.

We acquire more outcomes on images defiled by inhomogeneity in Fig 7, where columns I, II, III, IV, V, VI and VII show the consequences of the Chan-Vese [11], DRLS [12], LBF [22], LIF [24], VLSBCS [3], Zhang *et al.* [5] model and proposed method separately. Results show that proposed method has achieved better results than previous methods.

Table 2 shows the time and repetitions of every strategy dependent on Fig 7. It is clear in Table 2 that, Chan-Vese took

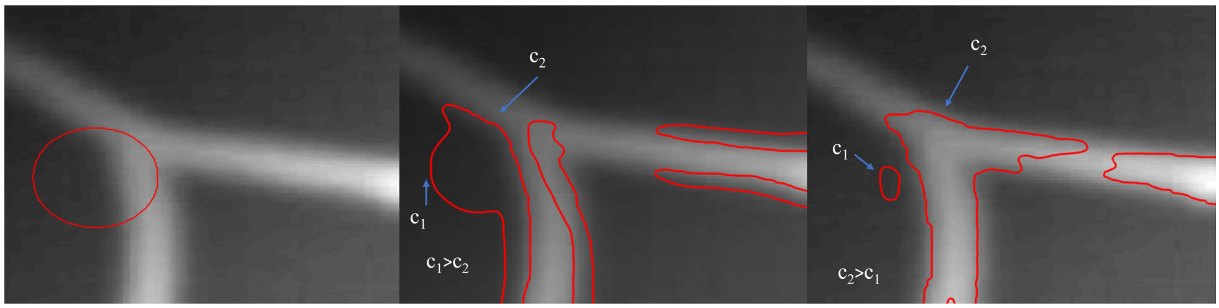

FIGURE 2. Effect of the swap function over local force terms. Column I: (Initialization contour), Column II: (Local term without swap function), III: (local terms after swap function).

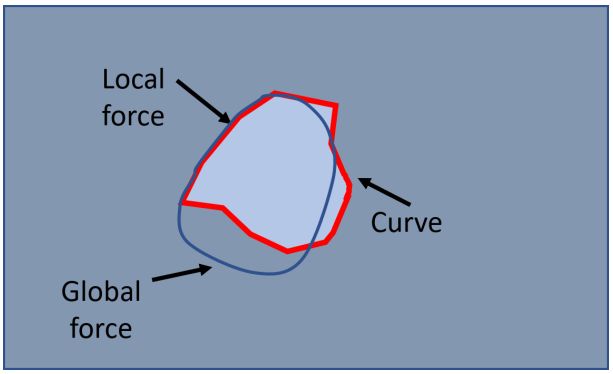

FIGURE 3. The intermingling of two forces: a: a global force moves contour towards boundary; b: The local energy captures inhomogeneous regions.

less time and cycles contrasted with past techniques, in any case, this strategy isn't able to yield precise outcomes. However, Proposed technique have delivered precise outcomes with second least number of cycles and time.

In Fig 8, one image is taken by changing its level of inhomogeneity from low to high. The consequences of the Chan-Vese [11], DRLS [12], LBF [22], LIF [24], VLSBCS [3], Zhang *et al.* [5] and proposed strategy are shown in columns I, II, III, IV, V, VI and VII. Results show that as the degree of inhomogeneity expands the past techniques surrender and perform incorrect image segmentation, while proposed strategy keeps up its strength and performs precise segmentation. Computational time and number of cycles taken for Fig 5 are appeared in Table 3, where Chan-Vese [11] didn't yield precise outcomes yet devoured least time. However, proposed strategy devoured fewer cycles and CPU time contrasted with past technique aside from Chan-Vese [11] and delivered precise outcomes.

Fig 9 gives result on some real images taken from publicly available sources. Results and its correlations are exhibited in I: (Chan-Vese [11]), II: (DRLS [12]), III: (LBF [22]), IV: (LIF [24]), V: (VLSBCS [3]), VI: (Zhang *et al.* [5]) and VII: (proposed technique) separately. Results determine the shortcomings of the past strategies, where Chan-Vese and DRLS techniques cannot get precise outcomes in appearance of inhomogeneity. LBF and LIF techniques are delicate to

TABLE 2. Time consumption and iterations of previous methods and proposed method in Fig 7.

Methods		a	b	c
Chan-Vese [11]	Iterations	**20**	**20**	**20**
	CPU time(sec)	**3.564**	**3.985**	**4.125**
DRLS [12]	Iterations	290	290	290
	CPU time(sec)	21.797	8.541	6.339
LBF [22]	Iterations	60	60	60
	CPU time(sec)	12.658	10.857	8.954
LIF [24]	Iterations	400	400	400
	CPU time(sec)	17.657	6.128	7.147
VLSBCS. [3]	Iterations	30	30	50
	CPU time(sec)	3.968	5.785	7.258
Zhang et al. [5]	Iterations	100	100	100
	CPU time(sec)	17.857	8.015	6.927
Proposed method	Iterations	50	50	50
	CPU time(sec)	4.985	3.874	5.254

position of initial curve, therefore these strategies yield false results. VLSBCS technique performed well and get precise outcomes at times, Zhang *et al.* [5] did not admirably performed as well. Therefore, the proposed strategy has outperformed past techniques and accomplished the required segmentation accurately.

We have counted the time consumption and cycles of every technique in Table 4 from Fig 9. The result of the proposed strategy is discrete as far as CPU time and cycles contrasted with past techniques.

V. KERNEL-BASED FUZZY C-MEANS CLUSTERING AND THRESHOLDING FOLLOWED BY PROPOSED METHOD

In traditional FCM [13], [14], the scope of each class is evaluated to minimize the cost function and it has been widely used in medical image segmentation algorithms. Recently, several methods have used FCM technique to automate active contour procedures [15], [41] in their way. Inspired by these methods [15], [41], we have also adapted kernel based FCM and thresholding approach to automate our segmentation

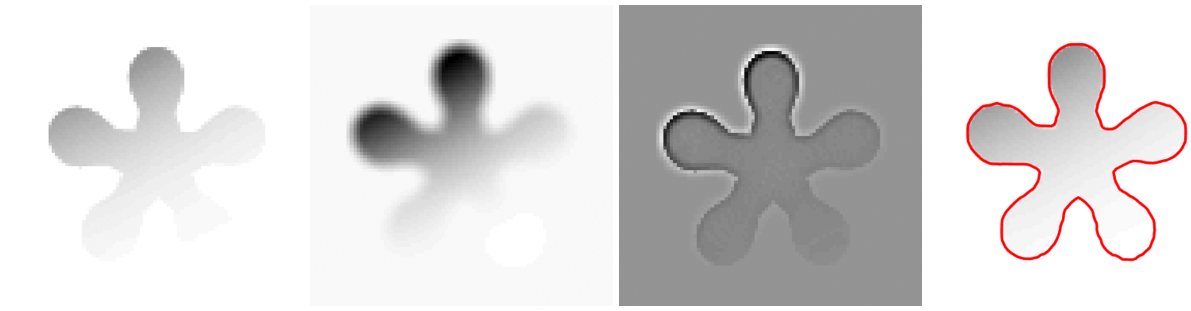

FIGURE 4. Proposed method result for inhomogeneous image a: Image. b: Bias estimation; c: Bias correction; d: Segmentation result.

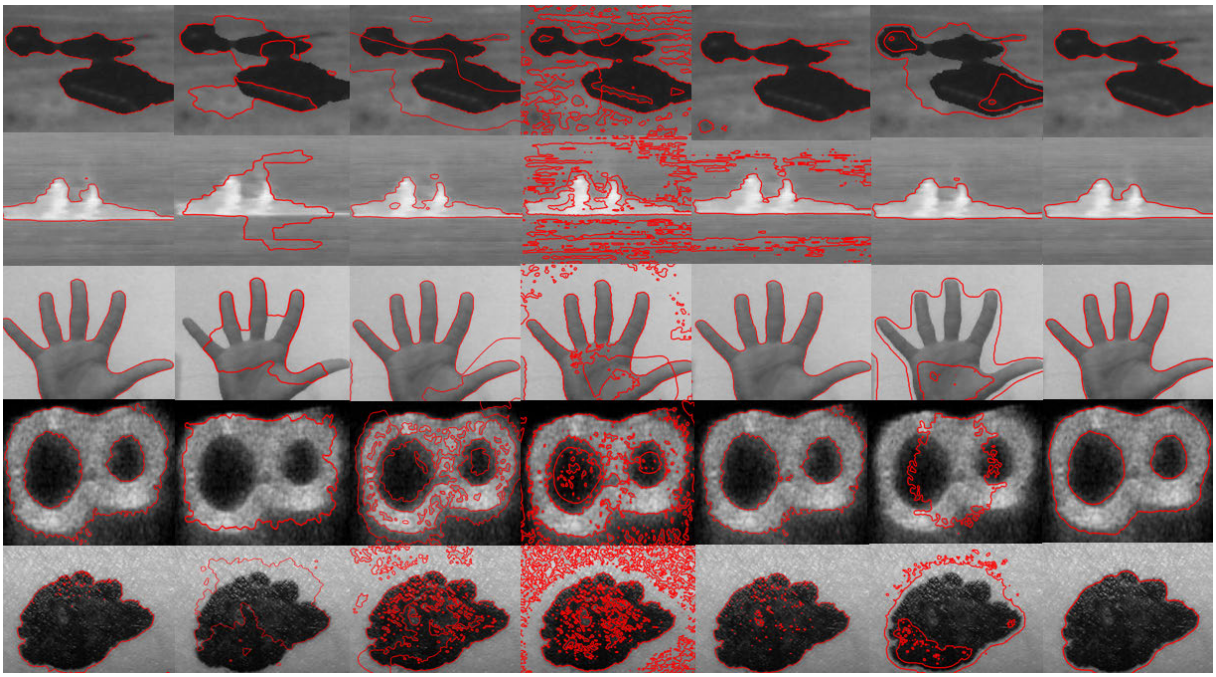

FIGURE 5. Proposed method result and its comparison. Column I: (Chan-Vese [11]), Column II: (DRLS [12]), III: (LBF [22]), IV: (LIF [24]), V: (VLSBCS [3]), VI: Zhang *et al.* [5] and VII: (proposed method) respectively.

FIGURE 6. Proposed method result and its comparison over real set of images. Column I: (Chan-Vese [11]), Column II: (DRLS [12]), III: (LBF [22]), IV: (LIF [24]), V: (VLSBCS [3]), VI: Zhang *et al.* [5] and VII: (proposed method) respectively.

method and to eradicate the problem of initial contour. We use, adaptive regularization for contextual information based on the heterogeneity factor of the grayscale intensity distribution. Moreover, a kernel window function is utilized instead of the Euclidean distance metric to increase segmentation accuracy. Further, We use clustered images for

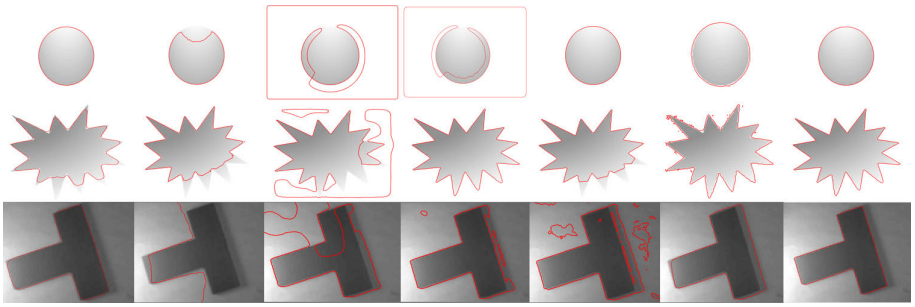

FIGURE 7. Comparison of the proposed method on different images from different modalities. Column I: (DRLS [12]), Column II: (Chan-Vese [11]), III: (LBF [22]), IV: (LIF [24]), V: (VLSBCS [3]), VI: Zhang *et al.* [5] and VII: (proposed method) respectively.

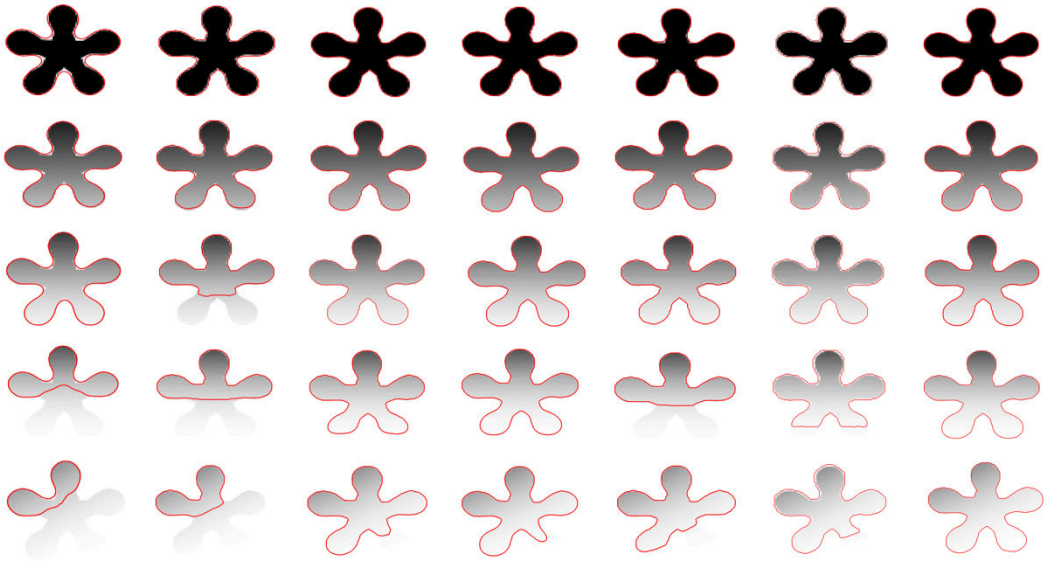

FIGURE 8. From low to severe intensity inhomogeneity comparison. Column I: (Chan-Vese [11]), Column II: (DRLS [12]), III: (LBF [22]), IV: (LIF [24]), V: (VLSBCS [3]), VI: Zhang *et al.* [5] and VII: (proposed method) respectively.

FIGURE 9. Comparison on real images with complicated intensity. Column I: (Chan-Vese [11]):, II: (DRLS [12]), III: (LBF [22]), IV: (LIF [24]), V: (VLSBCS [3]), VI: Zhang *et al.* [5] and VII: (proposed method).

binarization and perform intensity-based thresholding taken from [39], [40]. This scheme allows us to capture the desired region of interest by thresholding the image with a certain number of gray levels. It is very powerful preprocessing step, where the foreground and background of the object can be separated in multi-level of gray levels.

Traditional FCM techniques have used fixed statistical or pixel information for corresponding membership value,

TABLE 3. Time consumption and iterations taken by every method in Fig 8.

Methods		row 1	row 2	row 3	row 4	row 5
Chan-Vese [11]	Iterations	20	20	20	20	20
	CPU time(sec)	1.014	1.025	1.852	1.365	2.362
DRLS [12]	Iterations	250	250	250	250	250
	CPU time(sec)	6.579	6.579	6.472	6.039	6.335
LBF [22]	Iterations	20	20	20	30	50
	CPU time(sec)	4.325	4.254	4.857	4.958	9.241
LIF [24]	Iterations	500	500	500	500	700
	CPU time(sec)	3.254	3.754	3.857	4.014	4.852
VLSBCS. [3]	Iterations	50	50	50	200	200
	CPU time(sec)	2.758	2.897	3.965	4.325	4.254
Zhang et al. [5]	Iterations	100	100	100	100	100
	CPU time(sec)	3.365	12.254	11.852	21.875	24.965
Proposed method	Iterations	20	20	25	30	30
	CPU time(sec)	1.874	1.015	1.784	1.745	1.965

TABLE 4. Time consumption and iterations taken by every method in Fig 9.

Methods		row 1	row 2	row 3
Chan-Vese [11]	Iterations	250	1210	**610**
	CPU time(sec)	8.225	13.199	9.919
DRLS [12]	Iterations	**20**	**20**	**20**
	CPU time(sec)	**2.254**	**2.951**	**2.456**
LBF [22]	Iterations	100	100	100
	CPU time(sec)	13.754	12.657	11.967
LIF [24]	Iterations	500	500	500
	CPU time(sec)	18.752	16.965	17.652
VLSBCS. [3]	Iterations	30	30	30
	CPU time(sec)	7.354	4.254	6.742
Zhang et al. [5]	Iterations	50	50	50
	CPU time(sec)	16.325	10.875	8.965
Proposed method	Iterations	50	50	50
	CPU time(sec)	5.875	4.312	4.458

which is not appropriate because noise may differ within each local window. Subsequently, to get rid of this issue, this method uses an adaptive regularization parameter, which deals with spatial or contextual information. To do so, the local variation coefficient (LVC) is introduced to compute the inconsistency of the gray values within a local window. LVC is defined as:

$$(LVC)_i = \frac{\sum_{k\in N_i}\left(x_k - \overline{x_i}\right)^2}{N_R * \left(\overline{x_i}\right)^2} \tag{29}$$

where x_i is the grayscale pixel values around pixel i within local window N_i,N_r is cardinality and $\overline{x_i}$ is average of grayscale values. Furthermore, to acquire weights within the local window, exponential function is applied to LVC and ultimately weight is assigned to every pixel using

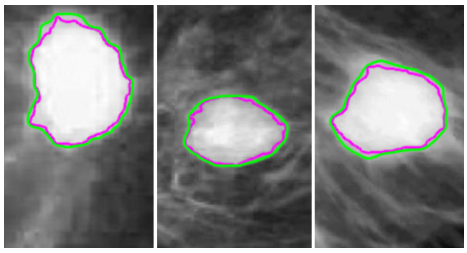

FIGURE 10. Result of the proposed method on Mammogram images taken from [47].

FIGURE 11. Result of the proposed method on real images taken from [46].

the following terms.

$$\zeta_i = \exp\left(\sum_{k\in N_i, i\neq k}(LVC)_k\right)$$
$$\omega = \frac{\zeta_i}{\sum_{k\in N_i}\zeta_k} \tag{30}$$
$$\varphi_i = \begin{cases} 2+\omega_i, \bar{x_i} < x_i \\ 2-\omega_i, \bar{x_i} > x_i \\ 0, \bar{x_i} = x_i \end{cases} \tag{31}$$

Further, (31) allocates large values for pixels with higher LVC values and similarly if the mean of local window grayscale is equal to the value of central pixel value, (31) will be zero and the algorithm will act as a normal FCM algorithm.

Finally, we perform the active contour segmentation over the images obtained from previous stage. We use the level set method proposed earlier in this research for final contouring. In the end, we compare ground truth with final result to validate our method. This process is shown in Fig 12.

VI. QUANTITATIVE COMPARISONS

For the quantitative results, this method presents segmentation of Mammogram images in Fig 10 taken from public dataset [47], the size of all images is 1024 × 1024. This presents the segmentation of mammogram tumor images (in pink) and manually annotated ground truths (in green). Further, we also took more real images from [46] dataset and the segmentation result of the proposed method is also shown in Fig 11 over some real images [46].

We process the Dice index, accuracy, sensitivity, specificity and Jaccard index metrics to analyze our technique

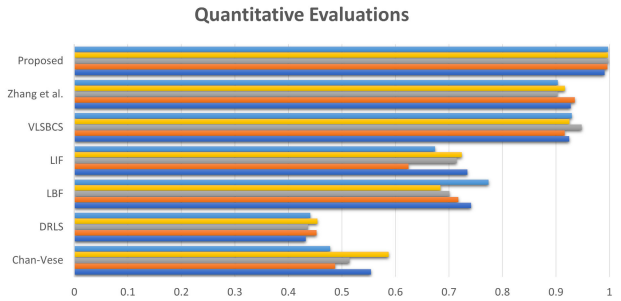

	Chan-Vese	DRLS	LBF	LIF	VLSBCS	Zhang et al.	Proposed
Jaccard	0.4782	0.4412	0.7741	0.6741	0.9297	0.9035	0.9976
Specificity	0.5874	0.4542	0.6841	0.7241	0.9254	0.9168	0.9974
Sensitivity	0.5141	0.4367	0.7012	0.7143	0.9482	0.9032	0.9981
Accuracy	0.4874	0.4528	0.7178	0.6245	0.9164	0.9354	0.9963
DSC	0.5542	0.4327	0.7415	0.7345	0.9247	0.9276	0.9912

FIGURE 12. Comparison of the proposed method with previous methods from Fig 10.

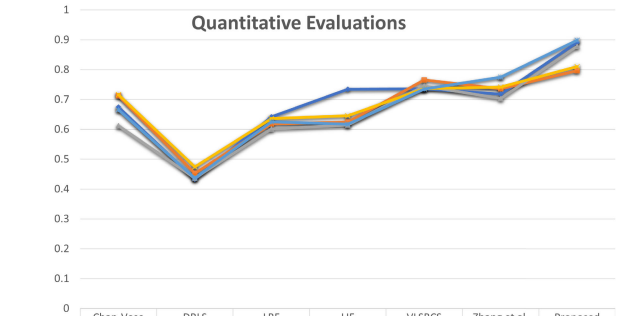

	Chan-Vese	DRLS	LBF	LIF	VLSBCS	Zhang et al.	Proposed
DSC	0.6745	0.4327	0.6415	0.7345	0.7354	0.7176	0.8912
Accuracy	0.7126	0.4528	0.6178	0.6245	0.7652	0.7354	0.7963
Sensitivity	0.6121	0.4367	0.6012	0.6143	0.7452	0.7032	0.8781
Specificity	0.7164	0.4741	0.6357	0.6452	0.7365	0.7417	0.8102
Jaccard	0.6654	0.4365	0.6251	0.6175	0.7347	0.7745	0.8985

FIGURE 13. Comparison of the proposed method with previous methods on real images from [46].

quantitatively. The acquired outcome will be considered acceptable when their values are near 1. Dice coefficient measures the amount of recognized tumor that matches the ground truth, sensitivity metric characterizes that every single recognized locale (tumors) are right and associated with the ground truth, accuracy metric explains the similarity of segmented part to ground truth, specificity is how accurately system avoids true negative regions and Jaccard index coefficient measures the overlap of result over ground truth.

$$DSC = \frac{2 \times TP}{2 \times TP + FP + FN} \tag{32}$$

$$Accuracy = \frac{TP + TN}{TP + TN + FP + FN}, \tag{33}$$

$$Sensitivity = \frac{TP}{TP + FN} \tag{34}$$

$$Specificity = \frac{(TN)}{(TN + FP)} \tag{35}$$

$$Jaccard = \frac{(TP)}{(FP + TP + FN)} \tag{36}$$

TP (true positive) relate to fragmented tumor tissues, TN (true negative) compare to accurately unsegmented tissues, FP (false positive) relate to the normal tissues considered wrongly as tumor tissues and FN (false negative) relate to the undetected tumor locales.

The quantitative analysis of Fig 10 is shown in Fig 12 and it shows that proposed strategy has accomplished better Dice index, accuracy, sensitivity, specificity and Jaccard index values contrasted with past strategies.

Similarly, the quantitative analysis of proposed method over caltech [46] dataset is shown in Fig 13 and it shows that proposed strategy has accomplished better average values of Dice index, accuracy, sensitivity, specificity and Jaccard index values contrasted with past strategies.

A. QUANTITATIVE VALIDATION ON BRATS DATASET

MRI (Magnetic Resonance Imaging) is viewed as the most generally utilized noninvasive methodology for brain tumor

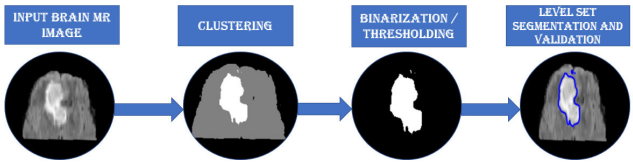

FIGURE 14. Proposed framework for brain MR tumor detection.

detection [44]. Detection of unusual regions in MRI is fundamental since it helps specialists and experts to examine the development of a tumor. Researchers have proposed numerous segmentation approaches for brain tumor detection. Active contours have been also associated with brain tumor detection [45]. Therefore, we have likewise proposed a technique on the BRATS 2015 test dataset [48]. This dataset contains four successions for every case known as T1-weighted(T1), T1 with gadolinium-upgrading contrast (T1c), T2-weighted (T2), and FLAIR. Proposed clustering-based approach has been executed over BRATS 2015 [48] dataset over 200 HGG(high-grade glioma) and 44 LGG(low-grade) patient volumes.

Fig 15 shows the segmentation result of proposed clustering based approach for brain tumor detection on few MR Images. We have also calculated average values of dice index, accuracy, sensitivity, specificity and Jaccard index metrics for the BRATS dataset as shown in Fig 16 and compared it with the previous state of the art active contour methods. From the results, we can deduce that proposed semi-automatic approach has captured desired output with increased quantitative values.

B. COMPARISON WITH EXISTING CLUSTERING MODELS

We have also evaluated and compared adaptive FCM rmethod with two popular clustering methods i-e spectral [43] and K-means [42] clustering. These methods are executed over skin lesion images and the captured results are evaluated by using ground truth. The results of adaptive FCM, K-means and spectral clustering on a single image are shown in 17,

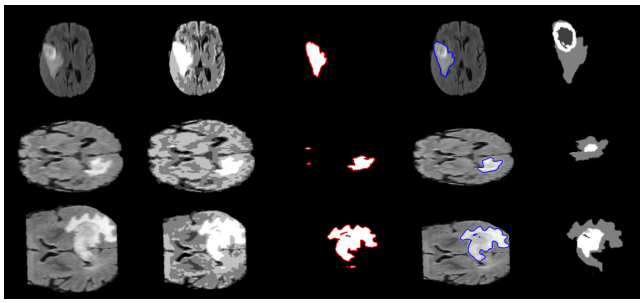

FIGURE 15. Proposed method for brain tumor detection. Column I: original image, II: clustering, III: thresholding, IV: final result, V: ground truth.

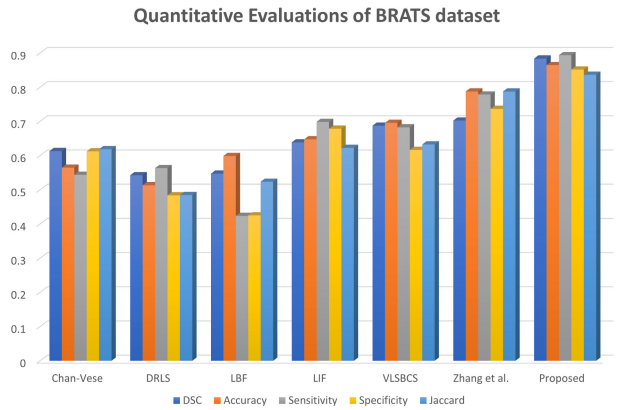

FIGURE 16. Quantitative results of the BRATS dataset and its comparison.

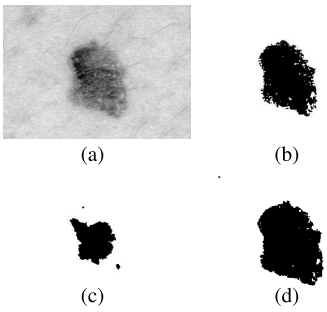

FIGURE 17. Comparison of clustering methods a: original image; b: Outcome of k-means clustering; c: Outcome of spectral clustering; d: Outcome of adaptive FCM.

which shows that adaptive FCM can distinguish boundaries better than previous approaches. We processed 30 images of the skin lesion dataset taken from [37] and compared quantitative results in 18 by using Jaccard, specificity, sensitivity, accuracy and DSC metrics explained in 36, 33, 34,35 and 32. The results have shown that adaptive FCM is robust and efficient compared to K-means and spectral clustering methods.

VII. DISCUSSION

A. TRAD-OFF BETWEEN THE LOCAL AND GLOBAL INFORMATION

Global information can only segment objects, which have only homogeneous region of pixels and these models

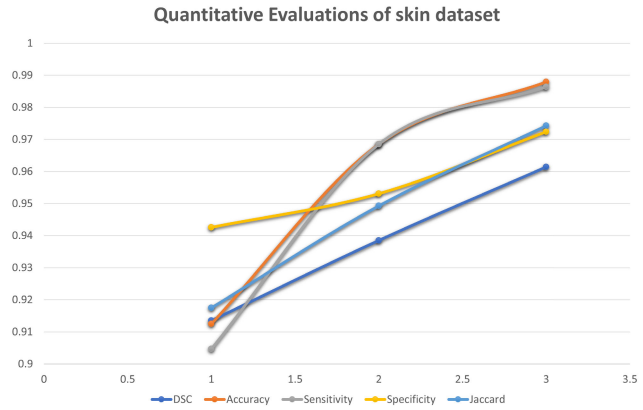

FIGURE 18. Quantitative validations of the clustering methods.

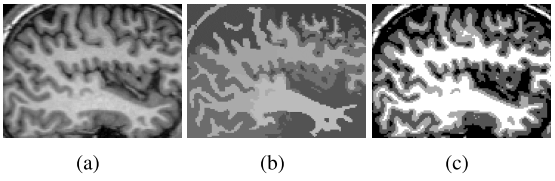

FIGURE 19. Euclidean distance metric and kernel window comparison a: original image; b: Outcome of FCM clustering with Euclidean distance metric; c: Outcome of adaptive FCM with kernel window function.

cannot provide subtle segmentation results with inhomogeneity. The local models can segment objects in the presence of inhomogeneity to some extent. However, local models alone are insufficient to carry out segmentation in a smooth way and often stuck into local minimum due to its sensitivity for contour initialization. Therefore, modern active contour methods are proposed on a hybrid strategy.

B. KERNEL FUNCTION vs. EUCLIDEAN DISTANCE METRIC

The traditional FCM method uses the Euclidean distance metric for partitioning data. However, this technique is proved to be sensitive to perturbations and outliers. Lately, a kernel trick has been utilized by Support vector machines where data could be partitioned with good accuracy [49]. Adaptive FCM also uses kernel based scheme to modify the behavior of the adaptive FCM as nonlinear. In this regard, we have illustrated the comparison of traditional FCM and Adaptive FCM in Fig 19 which uses kernel window function instead of Euclidean distance metric. The outcome of the Adaptive clustering demonstrates that kernel window function can preserve borders of data accurately compare to the traditional FCM method.

C. DIFFERENCE BETWEEN MACHINE LEARNING-BASED AND LEVEL SET BASED SEGMENTATION MODELS

Modern segmentation methods are also using machine learning [38], specifically deep learning based structure for object segmentation because of its accuracy and robustness. However, deep learning methods demand high cost resources and

prior knowledge of data, which may not available in all the cases. The proposed method uses a level set based partial differential structure, which does not require GPU, physical resources and any prior knowledge of data.

VIII. CONCLUSION

This research has proposed a novel hybrid model based on active contours. A hybrid force term of the local and global energy is proposed for inhomogeneous image segmentation. The adaptive force model is coordinated with the bias field, where a swap function was introduced to interchange local fitting terms to avoid level set evolution being stuck in a local minimum and produce wrong segmentation results. Moreover, the proposed technique has been extended and automated by integrating kernel-based fuzzy c-means clustering and thresholding as an initialization technique for the proposed method. In this way, we have eliminated the problem of contour initialization and its limitation for different applications. In this regard, we have conducted several experiments on images with various intensity variations. For quantitative approval, we have performed experiments over brain tumor images taken from the BRATS dataset and mammogram images from. Further, these results were evaluated using Dice index coefficient, accuracy, sensitivity, specificity and Jaccard index metric investigations. Results show that the proposed strategy has achieved better outcomes contrasted with past techniques, which has outperformed the restrictions of past global and local active contour techniques and expanded the proficiency of the proposed technique.

One of the bottlenecks of the local region based model is time complexity. Therefore, in our future work, we may eliminate the local force and enable the newly formulated method to capture objects using only the edge and semantic information of an image.

REFERENCES

[1] E. Ahmed, G. F. Georgy, S. Jasjit, and E. Ayman, "Medical image segmentation: A brief survey," in *Multi Modality State-of-the-Art Medical Image Segmentation Registration Methodologies*. Springer, 2011, pp. 1–39.

[2] U. Vovk, F. Pernus, and B. Likar, "A review of methods for correction of intensity inhomogeneity in MRI," *IEEE Trans. Med. Imag.*, vol. 26, no. 3, pp. 405–421, Mar. 2007.

[3] C. Li, R. Huang, Z. Ding, J. C. Gatenby, D. N. Metaxas, and J. C. Gore, "A level set method for image segmentation in the presence of intensity inhomogeneities with application to MRI," *IEEE Trans. Image Process.*, vol. 20, no. 7, pp. 2007–2016, Jul. 2011.

[4] C. Li, J. C. Gore, and C. Davatzikos, "Multiplicative intrinsic component optimization (MICO) for MRI bias field estimation and tissue segmentation," *Magn. Reson. Imag.*, vol. 32, no. 7, pp. 913–923, Sep. 2014.

[5] K. Zhang, L. Zhang, K.-M. Lam, and D. Zhang, "A level set approach to image segmentation with intensity inhomogeneity," *IEEE Trans. Cybern.*, vol. 46, no. 2, pp. 546–557, Feb. 2016.

[6] T. Ivanovska, R. Laqua, L. Wang, A. Schenk, J. H. Yoon, K. Hegenscheid, H. V. O. lzke, and V. Liebscher, "An efficient level set method for simultaneous intensity inhomogeneity correction and segmentation of MR images," *Comput. Med. Imag. Graph.*, vol. 48, pp. 9–20, Mar. 2016.

[7] M. Kass, A. Witkin, and D. Terzopoulos, "Snakes: Active contour models," in *Proc. 1st Int. Conf. Comput. Vis.*, vol. 259, 1987, p. 268.

[8] V. Caselles, R. Kimmel, and G. Sapiro, "Geodesic active contours," *Int. J. Comput. Vis.*, vol. 22, no. 1, pp. 61–79, 1997.

[9] C. Li, C. Xu, C. Gui, and M. D. Fox, "Level set evolution without re-initialization: A new variational formulation," in *Proc. IEEE Comput. Soc. Conf. Comput. Vis. Pattern Recognit. (CVPR)*, vol. 1, Jun. 2005, pp. 430–436.

[10] D. Mumford and J. Shah, "Optimal approximations by piecewise smooth functions and associated variational problems," *Commun. Pure Appl. Math.*, vol. 42, no. 5, pp. 577–685, 1989.

[11] T. F. Chan and L. A. Vese, "Active contours without edges," *IEEE Trans. Image Process.*, vol. 10, no. 2, pp. 266–277, Feb. 2001.

[12] C. Li, C. Xu, C. Gui, and M. D. Fox, "Distance regularized level set evolution and its application to image segmentation," *IEEE Trans. Image Process.*, vol. 19, no. 12, pp. 3243–3254, Dec. 2010.

[13] K. Chuang, H. Tzeng, L. Hong, S. Chen, J. Wu, and T. Chen, "Fuzzy *c*-means clustering with spatial information for image segmentation," in *Computerized Medical Imaging and Graphics*, vol. 30. Amsterdam, The Netherlands: Elsevier, 2006, pp. 09–15.

[14] W. Cai, S. Chen, and D. Zhang, "Fast and robust fuzzy c-means clustering algorithms incorporating local information for image segmentation," *Pattern Recognit.*, vol. 40, no. 3, pp. 825–838, Mar. 2007.

[15] B. N. Li, C. K. Chui, S. Chang, and S. H. Ong, "Integrating spatial fuzzy clustering with level set methods for automated medical image segmentation," *Comput. Biol. Med.*, vol. 41, no. 1, pp. 1–10, 2011.

[16] K. Zhang, L. Zhang, H. Song, and W. Zhou, "Active contours with selective local or global segmentation: A new formulation and level set method," *Image Vis. Comput.*, vol. 28, no. 4, pp. 668–676, 2010.

[17] S. Soomro, F. Akram, J. H. Kim, T. A. Soomro, and K. N. Choi, "Active contours using additive local and global intensity fitting models for intensity inhomogeneous image segmentation," *Comput. Math. Methods Med.*, vol. 2016, Oct. 2016, Art. no. 9675249.

[18] S. Soomro, A. Munir, and K. N. Choi, "Hybrid two-stage active contour method with region and edge information for intensity inhomogeneous image segmentation," *PLoS ONE*, vol. 13, no. 1, Jan. 2018, Art. no. e0191827.

[19] A. Munir, S. Soomro, C. H. Lee, and K. N. Choi, "Adaptive active contours based on variable kernel with constant initialisation," *IET Image Process.*, vol. 12, no. 7, pp. 1117–1123, Jul. 2018.

[20] S. Soomro, T. A. Soomro, and K. N. Choi, "An active contour model based on region based fitting terms driven by p-Laplace length regularization," *IEEE Access*, vol. 6, pp. 58272–58283, 2018.

[21] S. Soomro, F. Akram, A. Munir, C. H. Lee, and K. N. Choi, "Segmentation of left and right ventricles in cardiac MRI using active contours," *Comput. Math. Methods Med.*, vol. 2017, Aug. 2017, Art. no. 8350680.

[22] C. Li, C.-Y. Kao, J. C. Gore, and Z. Ding, "Minimization of region-scalable fitting energy for image segmentation," *IEEE Trans. Image Process.*, vol. 17, no. 10, pp. 1940–1949, Oct. 2008.

[23] L. Wang, L. He, A. Mishra, and C. Li, "Active contours driven by local Gaussian distribution fitting energy," *Signal Process.*, vol. 89, no. 12, pp. 2435–2447, Dec. 2009.

[24] K. Zhang, H. Song, and L. Zhang, "Active contours driven by local image fitting energy," *Pattern Recognit.*, vol. 43, no. 4, pp. 1199–1206, Apr. 2010.

[25] Y. Peng, F. Liu, and S. Liu, "Active contours driven by normalized local image fitting energy," *Concurrency Comput., Pract. Exper.*, vol. 26, no. 5, pp. 1200–1214, Apr. 2014.

[26] X. Xie, A. Zhang, and C. Wang, "Local average fitting active contour model with thresholding for noisy image segmentation," *Optik*, vol. 126, nos. 9–10, pp. 1021–1026, May 2015.

[27] X.-F. Wang, D.-S. Huang, and H. Xu, "An efficient local Chan–Vese model for image segmentation," *Pattern Recognit.*, vol. 43, no. 3, pp. 603–618, 2010.

[28] L. Wang, C. Li, Q. Sun, D. Xia, and C.-Y. Kao, "Active contours driven by local and global intensity fitting energy with application to brain MR image segmentation," *Comput. Med. Imag. Graph.*, vol. 33, no. 7, pp. 520–531, Oct. 2009.

[29] X. Li, D. Jiang, Y. Shi, and W. Li, "Biomedical engineering online," *Biomed. Eng.*, vol. 14, pp. 1–8, Jun. 2015.

[30] G. Liu, H. Li, and L. Yang, "A topology preserving method of evolving contours based on sparsity constraint for object segmentation," *IEEE Access*, vol. 5, pp. 19971–19982, 2017.

[31] H. Lv, Z. Wang, S. Fu, C. Zhang, L. Zhai, and X. Liu, "A robust active contour segmentation based on fractional-order differentiation and fuzzy energy," *IEEE Access*, vol. 5, pp. 7753–7761, 2017.

[32] S. Zhu, X. Bu, and Q. Zhou, "A novel edge preserving active contour model using guided filter and harmonic surface function for infrared image segmentation," *IEEE Access*, vol. 6, pp. 5439–5510, 2018.
[33] K. Zhang, Q. Liu, H. Song, and X. Li, "A variational approach to simultaneous image segmentation and bias correction," *IEEE Trans. Cybern.*, vol. 45, no. 8, pp. 1426–1437, Aug. 2015.
[34] C. Li, R. Huang, Z. Ding, C. Gatenby, D. Metaxas, and J. Gore, "A variational level set approach to segmentation and bias correction of images with intensity inhomogeneity," in *Proc. Int. Conf. Med. Image Comput. Comput.-Assist. Intervent.* Springer, 2008, pp. 1083–1091.
[35] Y. Wang and C. He, "Adaptive level set evolution starting with a constant function," *Appl. Math. Model.*, vol. 36, no. 7, pp. 3217–3228, 2012.
[36] G. Aubert and P. Kornprobst, "Mathematical problems in image processing: Partial differential equations and the calculus of variations," in *Springer Science and Business Media*, vol. 147. Springer, 2006.
[37] T. Mendonca, P. M. Ferreira, J. S. Marques, A. R. S. Marcal, and J. Rozeira, "PH2—A dermoscopic image database for research and benchmarking," in *Proc. 35th Annu. Int. Conf. IEEE Eng. Med. Biol. Soc. (EMBC)*, Jul. 2013, pp. 5437–5440.
[38] M. M. Abdelsamea and G. Gnecco, "Robust local–global SOM-based ACM," *Electron. Lett.*, vol. 51, no. 2, pp. 142–143, Jan. 2015.
[39] R. Saini and M. Dutta, "Image segmentation for uneven lighting images using adaptive thresholding and dynamic window based on incremental window growing approach," *Int. J. Comput. Appl.*, vol. 56, no. 13, pp. 31–36, Oct. 2012.
[40] J. Humayun, A. S. Malik, and N. Kamel, "Multilevel thresholding for segmentation of pigmented skin lesions," in *Proc. IEEE Int. Conf. Imag. Syst. Techn.*, May 2011, pp. 310–314.
[41] A. Elazab, C. Wang, F. Jia, J. Wu, G. Li, and Q. Hu, "Segmentation of brain tissues from magnetic resonance images using adaptively regularized kernel-based fuzzy-means clustering," *Comput. Math. Methods Med.*, vol. 2015, Dec. 2015, Art. no. 485495.
[42] M. E. Celebi, "Improving the performance of k-means for color quantization," *Image Vis. Comput.*, vol. 29, no. 4, pp. 260–271, Mar. 2011.
[43] J. Shi and J. Malik, "Normalized cuts and image segmentation," *IEEE Trans. Pattern Anal. Mach. Intell.*, vol. 22, no. 8, pp. 888–905, Aug. 2000.
[44] S. Bauer, R. Wiest, L.-P. Nolte, and M. Reyes, "A survey of MRI-based medical image analysis for brain tumor studies," *Phys. Med. Biol.*, vol. 58, no. 13, pp. R97–R129, Jul. 2013.
[45] E. Ilunga-Mbuyamba, J. G. Avina-Cervantes, A. Garcia-Perez, R. de Jesus Romero-Troncoso, H. Aguirre-Ramos, I. Cruz-Aceves, and C. Chalopin, "Localized active contour model with background intensity compensation applied on automatic MR brain tumor segmentation," *Neurocomputing*, vol. 220, pp. 84–97, Jan. 2017.
[46] G. Griffin, A. Holub, and P. Perona, "Caltech-256 object category dataset," California Inst. Technol., Pasadena, CA, USA, Tech. Rep., 2007.
[47] P. Suckling, "The mammographic image analysis society digital mammogram database," in *Digital Mammo*, vol. 1994. Amsterdam, The Netherlands: Elsevier, 1994, pp. 375–386.
[48] B. H. Menze *et al.*, "The multimodal brain tumor image segmentation benchmark (BRATS)," *IEEE Trans. Med. Imag.*, vol. 34, no. 10, pp. 1993–2024, Oct. 2015.
[49] T. Hofmann, B. Schölkopf, and A. J. Smola, "Kernel methods in machine learning," *Ann. Statist.*, vol. 36, pp. 1171–1220, Apr. 2008.

SHAFIULLAH SOOMRO (Member, IEEE) received the Bachelor of Engineering (B.E.) degree from QUEST, Nawabshah, Sindh, Pakistan, in 2008, the Master of Engineering (M.E.) degree from MUET, Jamshoro, Sindh, in 2014, and the Ph.D. degree in computer science from Chung-Ang University, Seoul, South Korea, in 2018. He is currently an Assistant Professor. His research interests include motion tracking, object segmentation, and 3D image recognition.

ASAD MUNIR (Member, IEEE) received the bachelor's degree in engineering sciences from the GIK Institute, Pakistan, in 2013, and the master's degree in computer science from Chung-Ang University, South Korea, in 2018. He is currently pursuing the Ph.D. degree with the Department of Industrial and Information Engineering, University of Udine, Italy. His research interests include object segmentation, object tracking, and person re-identification.

ASIF AZIZ (Member, IEEE) received the B.E. degree from Mehran UET, Jamshoro, Pakistan, in 2010, and the M.E. degree from MUET, Jamshoro, Pakistan, in 2015. He is currently pursuing the Ph.D. degree in application software with Chung-Ang University, Seoul, South Korea. His research interests include image segmentation, image recognition, and medical imaging.

TOUFIQUE AHMED SOOMRO (Member, IEEE) received the B.E. degree in electronic engineering from the Mehran University of Engineering and Technology, Pakistan, in 2008, and the M.Sc. degree in electrical and electronic engineering from Universiti Teknologi PETRONAS, Malaysia, in 2014. He is currently pursuing the Ph.D. degree with the School of Computing and Mathematics, Charles Sturt University, Australia. He is also currently implementing software-based algorithm for the detection of eye-related disease. His research interests include most aspects of image enhancement and image analysis for medical images.

KWANG NAM CHOI (Member, IEEE) received the B.S. and M.S. degrees from the Department of Computer Science, Chung-Ang University, Seoul, South Korea, in 1988 and 1990, respectively, and the Ph.D. degree in computer science from the University of York, U.K., in 2002. He is currently a Professor with the School of Computer Science and Engineering, Chung-Ang University. His research interests include motion tracking, object categorization, and 3D image recognition.